Title

Evaluation of Particle Size Distribution Metrics to Estimate the Relative Contributions of Different Size Fractions Based on Measurements in Arctic Waters

Journal

Journal of Geophysical Research - Oceans, 125(6)

ISSN

2169-9275

Authors

Runyan, Hugh

Reynolds, Rick A

Stramski, Dariusz

Publication Date

2020-06-01

DOI

10.1029/2020jc016218

JGR Oceans

RESEARCH ARTICLE
10.1029/2020JC016218

Evaluation of Particle Size Distribution Metrics to Estimate the Relative Contributions of Different Size Fractions Based on Measurements in Arctic Waters

Hugh Runyan[1], Rick A. Reynolds[1], and Dariusz Stramski[1]

[1]Marine Physical Laboratory, Scripps Institution of Oceanography, University of California San Diego, La Jolla, CA, USA

Key Points:
- Measurements of Arctic seawater are used to examine variability in the shape of the size distribution of suspended particles
- A power law model performs poorly in predicting the relative contributions of three size classes to the particle size distribution
- Specific percentiles of the cumulative number, area, and volume distributions are strongly correlated with size class contributions

Correspondence to:
R. A. Reynolds,
rreynolds@ucsd.edu

Citation:
Runyan, H., Reynolds, R. A., & Stramski, D. (2020). Evaluation of particle size distribution metrics to estimate the relative contributions of different size fractions based on measurements in Arctic waters. *Journal of Geophysical Research: Oceans*, *125*, e2020JC016218. https://doi.org/10.1029/2020JC016218

Received 6 MAR 2020
Accepted 22 APR 2020
Accepted article online 5 MAY 2020

Abstract The size distribution of suspended particles influences several processes in aquatic ecosystems, including light propagation, trophic interactions, and biogeochemical cycling. The shape of the particle size distribution (PSD) is commonly modeled as a single-slope power law in oceanographic studies, which can be used to further estimate the relative contributions of different particle size classes to particle number, area, and volume concentration. We use a data set of 168 high size-resolution PSD measurements in Arctic oceanic waters to examine variability in the shape of the PSD over the particle diameter range 0.8 to 120 μm. An average value of -3.6 ± 0.33 was obtained for the slope of a power law fitted over this size range, consistent with other studies. Our analysis indicates, however, that this model has significant limitations in adequately parameterizing the complexity of the PSD, and thus performs poorly in predicting the relative contributions of different size intervals such as those based on picoplankton, nanoplankton, and microplankton size classes. Similarly, median particle size was also generally a poor indicator of these size class contributions. Our results suggest that alternative percentile diameters derived from the cumulative distribution functions of particle number, cross-sectional area, and volume concentration may provide better metrics to capture the overall shape of the PSD and to quantify the contributions of different particle size classes.

Plain Language Summary The particle size distribution (PSD) describes how the concentration of particles changes with particle size, and it is an important characteristic of suspended oceanic particles that influences ocean ecology and biogeochemistry. We collected an extensive set of measurements of the PSD from Arctic waters to examine how different size classes of particles contribute to the total concentration of particle number, cross-sectional area, and volume. A model of the PSD frequently employed for oceanic studies is found to have strong limitations in representing these measurements of natural samples, and consequently performs poorly in estimating the relative contributions of individual size classes. We show that an alternative approach of describing the PSD based on specific percentile diameters derived from the cumulative distribution function of size-dependent particle concentration provides a better means to characterize the shape of the PSD for oceanic particle assemblages and provides superior performance in estimating size class contributions.

1. Introduction

Suspended particles in seawater play a key role in mediating numerous biogeochemical and ecological processes within the ocean. An important characteristic of these assemblages is the particle size distribution (PSD), which quantifies the concentration of particles as a function of particle size. Knowledge of the PSD and other particle characteristics such as composition or shape is needed for understanding numerous physical, chemical, and biological processes that involve particles. Examples of such size-dependent processes include rates of particle aggregation and sinking (Burd, 2013; Jackson, 1995; Stemmann et al., 2004), particle colonization and remineralization rates (Kiørboe, 2000; Kiørboe et al., 2004; Ploug & Grossart, 2000), and planktonic metabolic processes and trophic interactions (Brown et al., 2004; Chisholm, 1992; Gillooly et al., 2001; Hansen et al., 1997; Jennings & Warr, 2003; Woodward et al., 2005). The PSD also plays a critical role in determining the light scattering and absorption properties of seawater, and thus the penetration of light within the ocean (Agagliate et al., 2018; Baker & Lavelle, 1984; Morel & Bricaud, 1986; Stemmann & Boss, 2012; Stramski et al., 2001; Stramski & Kiefer, 1991).

Table 1
List of Notation

Symbol	Description, [typical units]
D	Equivalent spherical diameter, [μm]
$N(D)$, $A(D)$, $V(D)$	Particle size distribution based on number, cross-sectional area, or volume concentration, [m^{-3}, $\mu m^2\ m^{-3}$, or $\mu m^3\ m^{-3}$]
$N'(D)$, $A'(D)$, $V'(D)$	Density functions of $N(D)$, $A(D)$, or $V(D)$, [$m^{-3}\ \mu m^{-1}$, $\mu m^2\ m^{-3}\ \mu m^{-1}$, $\mu m^3\ m^{-3}\ \mu m^{-1}$]
N_t, A_t, V_t	Total concentration of particle number, area, or volume over size range D = 0.8 to 120 μm, [m^{-3}, $\mu m^2\ m^{-3}$, $\mu m^3\ m^{-3}$]
$\zeta_{(N, A, or V)}$	Slope of power law fit to $N'(D)$, $A'(D)$, or $V'(D)$, [unitless]
$CDF_{(N, A, or V)}(D)$	Cumulative distribution function of $N'(D)$, $A'(D)$, or $V'(D)$, [unitless]
$D_{(N, A, or V)}(X)$	Diameter corresponding to the X^{th} percentile value of $CDF_N(D)$, $CDF_A(D)$, or $CDF_V(D)$, [μm]
$f_{(N, A, or V), (pico, nano, or micro)}$	Fractional contribution to N_t, A_t, or V_t of the picoplankton, nanoplankton, or microplankton size class, [unitless]

Note. Symbols appearing with a hat above them, e.g., $\hat{f}$, indicate a model-derived value.

The PSD can be defined as the numerical concentration of particles per unit particle size interval, denoted here by $N'(D)$ and expressed in units of $m^{-3}\ \mu m^{-1}$ (Jonasz & Fournier, 2007):

$$N(D)=N'(D)\,\Delta D, \tag{1}$$

where $N(D)$ is the number of particles per unit volume (m^{-3}) in the size interval $D \pm 0.5\Delta D$, and D is the midpoint diameter of each size class in μm (see also Table 1 for a list of notation used throughout the paper). Depending on the technique of size measurement, the particle diameter typically represents the volume-equivalent or area-equivalent spherical diameter. The number-based distribution, $N(D)$, can be transformed to other distributions based on the concentration of particle cross-sectional area, $A(D)$, or volume, $V(D)$, through assumptions of particle shape such as a sphere. To account for variations in the width of measured size intervals, the different forms of PSD or density functions, $N'(D)$, $A'(D)$, and $V'(D)$, are calculated by dividing the respective values of $N(D)$, $A(D)$, and $V(D)$ for each size bin by its width.

The size distribution of marine particle assemblages is continually varying in time and space as several competing processes add or remove particles from a given volume of seawater, or by conversions of particles from one type to another which are accompanied by changes in particle size. Characterizing and predicting variability in the PSD of oceanic waters is thus a major research challenge. Recent advances in particle imaging and other optically-based measurement technologies based on light scattering including diffraction have increased capabilities to measure the PSD in oceanic waters (Agrawal & Pottsmith, 2000; Graham & Nimmo-Smith, 2010; Jackson et al., 1997; Moore et al., 2009; Picheral et al., 2010), but in situ measurements alone cannot provide the spatial or temporal resolution needed to characterize global oceanic ecosystems. For this reason, efforts to develop remote-sensing approaches for estimation of the PSD from airborne or satellite measurements of ocean color have been pursued (Bowers et al., 2007; Kostadinov et al., 2009; Shi & Wang, 2019). These approaches generally rely on empirical parameterizations or simplified descriptions of the PSD in order to quantify relationships between the PSD and the optical properties of seawater.

Single metrics such as the mean or median particle diameter derived from the distribution of particle number, area, or volume concentration are one means to characterize the PSD (Bernard et al., 2007; Briggs et al., 2013; Slade & Boss, 2015; Woźniak et al., 2010). Alternatively, parametrizations that describe the shape of the PSD in seawater have also been proposed, such as power law models (Bader, 1970), Gaussian or log-normal distributions (Jonasz, 1983, 1987), and the gamma function (Risović, 1993). The power law model, often referred to as the Junge distribution, is the most commonly utilized and previous studies have offered justification for its applicability to marine assemblages (Kiefer & Berwald, 1992; Platt & Denman, 1978; Sheldon et al., 1972). The density function of particle number concentration for this model can be written as

$$N'(D)=N'_o\,(D/D_o)^{\zeta_N} \tag{2}$$

where D_o is a reference diameter (μm), N'_o ($m^{-3}\ \mu m^{-1}$) is the value at D_o, and ζ_N is the dimensionless

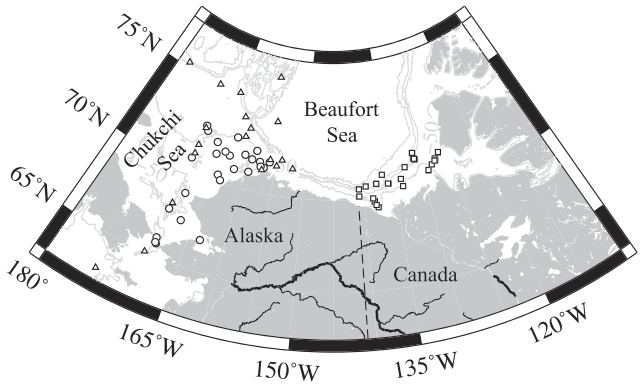

Figure 1. Map of study area depicting sampling locations for the MALINA (□), ICESCAPE (○), and Mirai (△) cruises.

slope of the distribution. Reported values for ζ_N in oceanic waters span a wide range and can vary for different size regions of the PSD (Jonasz & Fournier, 2007), but the majority of observations fall in the range of −4 to −3 (Buonassissi & Dierssen, 2010; Reynolds et al., 2010, 2016; Xi et al., 2014).

Although planktonic organisms exhibit a continuum of sizes, it has long been recognized that different particle size ranges tend to have different physiological capabilities as well as different ecological and biogeochemical roles (Le Quéré et al., 2005; Stemmann & Boss, 2012; Ward et al., 2012). The PSD is thus often further aggregated into broad size classes representing different planktonic "functional types" based on characteristic cell size (IOCCG, 2014; Mouw et al., 2017). The most common size grouping of plankton used in pelagic studies includes three planktonic size classes based on particle diameter (Sieburth et al., 1978); picoplankton (diameter range 0.2–2 μm), nanoplankton (2–20 μm), and microplankton (20–200 μm). Estimation of the relative contributions of these three size classes to the PSD is commonly used in ecological studies and its determination from remote sensing is also a subject of recent research efforts (IOCCG, 2014; Kostadinov et al., 2010).

Observations in various marine environments suggest that the PSD often exhibits a complex shape in response to the varying physical and biological processes that operate in aquatic ecosystems (Jonasz & Fournier, 2007; Reynolds et al., 2010; Sheldon et al., 1972), which reduces the ability of single descriptors of the size distribution to accurately quantify the role of different size ranges. The main objectives of this study are to evaluate variability in the relative contributions of different size classes to the particle number, area, and volume concentration and to explore the utility of relatively simple measures derived from the generally complex shapes of the measured PSD to estimate these contributions. For this purpose, we utilize 168 measurements of PSDs collected at 87 sites in the Arctic Ocean to characterize the shape of the PSD and the contribution of different particle size classes to overall particle number, area, and volume concentrations. These measurements, obtained with an electrical impedance approach (Coulter Counter), provide high size resolution measurements of the PSD for particle diameters spanning the range from 0.8 to 120 μm, enabling calculation of the relative contribution of particles in different size classes to total particle concentration. These size intervals were chosen to approximate the picoplankton, nanoplankton, and microplankton size range. We compare the measured particle number distributions with the single-slope power law parametrization and evaluate this model's capability to quantify the relative contributions of these three size classes. We then examine relationships between these size fraction contributions and the median and other percentile diameters derived from the cumulative distribution functions of particle number, area, and volume concentration.

2. Materials and Methods

2.1. Study Area and Sampling

Measurements were obtained on four expeditions to the western Arctic Ocean. The MALINA (MAckenzie LIght aNd cArbon) cruise occurred in the southeastern Beaufort Sea from 31 July to 24 August 2009 on the CCGS Amundsen. The station grid bracketed the outflows of the Mackenzie River, with transects extending from the delta to the southernmost limit of the pack ice outside the continental shelf. Two cruises associated with the NASA ICESCAPE (Impacts of Climate on EcoSystems and Chemistry of the Arctic Pacific Environment) program utilized the USCGC Healy to sample the Chukchi Sea and western Beaufort Sea during two successive years; from 18 June through 16 July 2010 and from 28 June through 24 July 2011. Sampling on these cruises included transects where measurements were done from open water across the ice edge to several kilometers within consolidated pack ice. A fourth cruise took place onboard the RV Mirai from 26 August to 18 September 2017 as part of the Japanese ArCS (Arctic Challenge for Sustainability) program, with sampling conducted from the Bering Strait to the southern limit of the ice edge at about 76.5°N. From these four cruises, 168 samples were collected for measurements of the PSD (Figure 1).

Water samples were obtained from two or three depths at each station using a CTD-Rosette equipped with Niskin bottles. The near surface layer (nominally 1–3 m depth) was always sampled, with additional depths corresponding to features such as maxima in chlorophyll *a* fluorescence or the optical beam attenuation coefficient, turbid layers within 3–5 m above the bottom on the shelf, or depths up to 300 m offshore. Water from an entire Niskin bottle or combination of bottles was withdrawn by opening the bottom closure and draining the contents into 20-L carboys to ensure collection of all particles and to minimize sampling error related to particle settling within the bottle. All measurements were made on board the research vessels and began within 1 hr of sampling.

2.2. Measurements of the PSD

The PSD was measured on seawater samples using a Coulter counter, an instrument that has been used for decades in the study of oceanic PSDs (Brun-Cottan, 1971; Carder et al., 1971; Jackson et al., 1997; Jonasz, 1983; Kitchen et al., 1975; Parsons, 1969; Sheldon et al., 1972). Water samples were withdrawn from the carboy after mixing, and the PSD was measured with a Beckman-Coulter Multisizer III using 0.2-μm filtered seawater as the diluent and blank. Samples were measured with a combination of two aperture sizes (30 and 200 μm), which provided the capability to count particles in the size range $D = 0.7$ to 120 μm where D represents volume equivalent spherical diameter. Both apertures were calibrated using suspensions of NIST-traceable microsphere standards of known size. For each seawater sample, multiple (>25) replicate measurements of the PSD were acquired for each aperture size and summed together to increase sampling volume and reduce the statistical error of particle counts. Total sample volumes after this summation averaged about 1.2 cm^3 for the 30-μm aperture and 180 cm^3 for the 200-μm aperture.

Each measurement with a given aperture provided the number of particles per unit volume, N (m^{-3}), within discrete size bins. Size classes consisted of 256 bins with logarithmically increasing bin width over the measured range of each aperture, ensuring high size resolution. The density function of the number concentration as a function of diameter, $N'(D)$ (m^{-3} μm^{-1}), was calculated by dividing the concentration of particles within each size bin by the bin width. To create the final distribution, measurements of $N'(D)$ from both apertures were merged at an overlapping size bin that shared a similar midpoint and bin width ($D = 4.8 \pm 0.03$ μm). The magnitude of $N'(D)$ as determined by the 30-μm aperture was adjusted to match the value measured by the 200-μm aperture at this overlapping bin, and the resulting merged distribution was converted back to $N(D)$ through multiplication of $N'(D)$ for each bin by the bin width. Because of high noise levels often observed with the smallest size bins of the 30-μm aperture, the distributions were truncated to a lower limit of $D = 0.8$ μm. The final merged distributions consist of 383 size bins spanning the range of D from 0.8 to 120 μm, with bin widths varying from about 0.01 to 1.6 μm.

2.3. Measurements of Particle Mass Concentration

Measurements of the particle dry mass concentration and organic carbon content were also obtained from the same samples to further characterize the bulk particle assemblage. The mass concentration of dried suspended particulate matter per unit volume of water, SPM (g m^{-3}), was measured using a standard gravimetric technique (van der Linde, 1998). Particles were collected on prerinsed, precombusted 25-mm glass-fiber filters (Whatman GF/F) that were weighed prior to use. Following filtration under low vacuum, sample filters and edges were rinsed with deionized water to remove residual sea salt, dried at 60°C, and stored sealed until analysis. The mass of particles collected on the filters was determined with a Mettler-Toledo MT5 microbalance with 1-μg precision. Two to three replicate filters were typically measured for each sample and averaged.

The concentration of particulate organic carbon, POC (mg m^{-3}), was obtained using a method consistent with established protocols (e.g., Knap et al., 1996). Water samples were filtered through precombusted 25-mm GF/F filters; filters were transferred to clean glass scintillation vials and dried at 60°C, then stored until post cruise analysis. Prior to analysis, filters were exposed to concentrated acid fumes (HCl) to remove inorganic carbon, and organic carbon concentration of each filter was determined with standard CHN analysis involving high temperature combustion of sample filters (Parsons et al., 1984). For MALINA, POC was measured from combustion of the same filters used in SPM determination. A number of unused filters from each lot of precombusted filters were used to quantify the background carbon content of filters and subtracted from the sample data. These blank filters were treated exactly like sample filters except that no

sample water was passed through them. Sample filtration volumes were large enough to ensure that contributions of the blank filter or adsorbed DOC were small relative to the particulate carbon content of the sample filter. Duplicate or triplicate samples were taken for each station and averaged to produce the final result of POC.

2.4. Analysis of Measured PSDs

The concentrations of particle cross-sectional area, $A(D)$ ($\mu m^2\ m^{-3}$), and particle volume, $V(D)$ ($\mu m^3\ m^{-3}$), within each size bin were calculated from the final merged $N(D)$ by assuming spherical particles and the relations $A(D) = N(D)\ \pi D^2/4$ and $V(D) = N(D)\ \pi D^3/6$. Density functions in terms of particle area concentration, $A'(D)$ ($\mu m^2\ m^{-3}\ \mu m^{-1}$), and particle volume concentration, $V'(D)$ ($\mu m^3\ m^{-3}\ \mu m^{-1}$), were computed in a manner similar to that of $N'(D)$ by dividing each value of $A(D)$ and $V(D)$ by the bin width.

To characterize the PSDs, cumulative distribution functions for particle number, $CDF_N(D)$, area, $CDF_A(D)$, and volume, $CDF_V(D)$, concentrations were calculated from the respective density functions, $N'(D)$, $A'(D)$, and $V'(D)$. For example, in the case of the particle number concentration, the cumulative distribution function $CDF_N(D)$ was computed according to

$$CDF_N(D) = \int_{0.8}^{D} N'(D)dD \Big/ \int_{0.8}^{120} N'(D)dD, \tag{3}$$

where the integration limits represent D in μm. The $CDF_A(D)$ and $CDF_V(D)$ functions were calculated in an analogous manner by replacing $N'(D)$ in equation 3 with $A'(D)$ and $V'(D)$, respectively. The particle diameters corresponding to specific percentiles of the cumulative distribution functions for particle number, area, and volume concentrations were then determined for each sample. The integral in the denominator of equation 3 is equivalent to the total particle number concentration over the measured size range of 0.8 to 120 μm, N_t (m^{-3}). Similarly, the total concentrations of particle area, A_t ($\mu m^2\ m^{-3}$), and volume, V_t ($\mu m^3\ m^{-3}$), can be calculated using the expression in the denominator of equation 3 and replacing $N'(D)$ with $A'(D)$ and $V'(D)$, respectively.

Other metrics characterizing the relative shapes of the PSDs were calculated by quantifying the fractional contributions of discrete size ranges to the values of N_t, A_t, and V_t. The size ranges of these classes were chosen to approximate the traditional plankton size classification scheme of Sieburth et al. (1978); picoplankton (f_{pico}; $0.8 \le D \le 2$ μm), nanoplankton (f_{nano}; $2 < D \le 20$ μm), and microplankton (f_{micro}; $20 < D \le 120$ μm). The fractional contributions of these size classes to the total number concentration were calculated according to

$$f_{N,pico} = \int_{0.8}^{2} N'(D)dD \Big/ \int_{0.8}^{120} N'(D)dD, \tag{4a}$$

$$f_{N,nano} = \int_{2}^{20} N'(D)dD \Big/ \int_{0.8}^{120} N'(D)dD, \tag{4b}$$

$$f_{N,micro} = \int_{20}^{120} N'(\mathrm{D})dD \Big/ \int_{0.8}^{120} N'(D)dD. \tag{4c}$$

The contributions of the three size classes to the particle area and volume distributions were calculated in an analogous manner by replacing $N'(D)$ in equation 4a-4c with $A'(D)$ and $V'(D)$, respectively. These fractional contributions are closely tied to the cumulative distribution functions described above. For example, equation 4a is equivalent to the cumulative distribution function of number concentration provided in equation 3 with an upper integration limit of $D = 2$ μm for the numerator. Similarly, the other size classes can be related to the CDF_N through the relations $f_{N,micro} = 1 - CDF_N(D = 20\ \mu m)$ and $f_{N,nano} = CDF_N(D = 20\ \mu m) - CDF_N(D = 2\ \mu m)$.

A final means to characterize the overall size distribution was determined by fitting a power law model to the measured data of the density function of particle number concentration (equation 2). This calculation was performed as a linear fit to $\log_{10}$-transformed data of $N'(D)$ and D over the entire measured size range. Prior to fitting, size bins for the 200-μm aperture that exhibited counts fewer than 20 particles (generally size bins corresponding to the largest diameters) were aggregated until that threshold was reached. We use the symbol $\hat{N}(D)$ to indicate the fitted values of the density function of particle number concentration. The

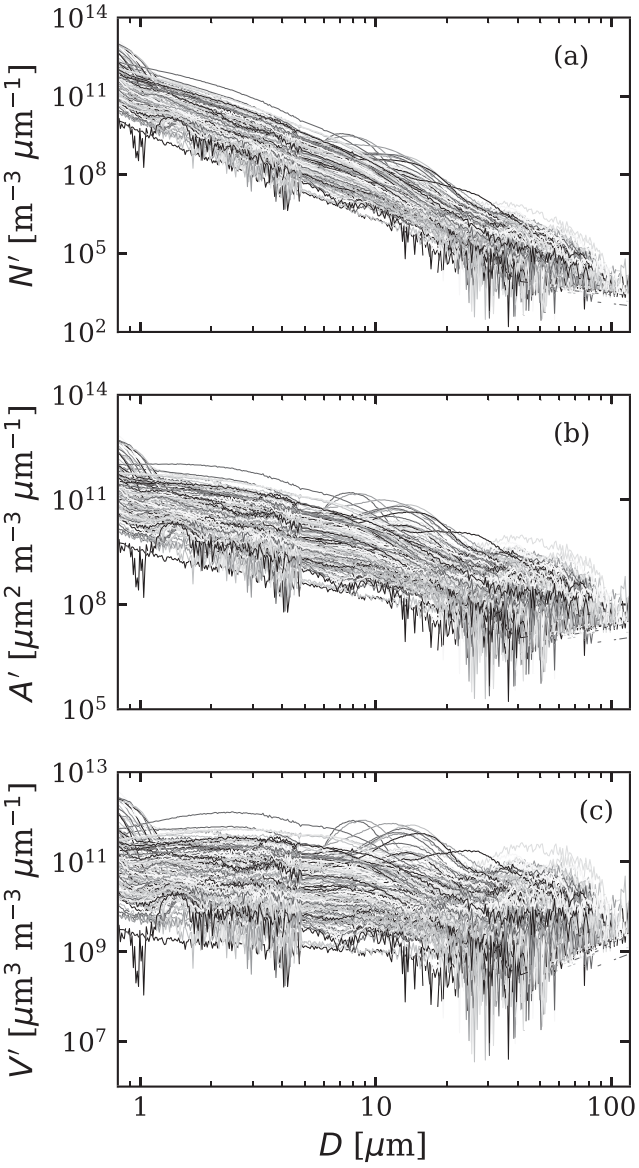

Figure 2. Measured density functions for the concentration of particle (a) number, N', (b) cross-sectional area, A', and (c) volume, V', as a function of equivalent spherical diameter D.

fitted power law functions of $\hat{A}'(D)$ and $\hat{V}'(D)$ were derived in a similar manner except that $A'(D)$ and $V'(D)$ replaced $N'(D)$, and ζ_A and ζ_V replaced ζ_N, in equation 2.

2.5. Statistical Analyses

We evaluated the capability of different metrics derived from the measured PSDs to estimate the fractional contributions of the picoplankton, nanoplankton, and microplankton size classes. Model I regression analysis was used to parameterize linear relationships, and nonlinear relationships were determined using the Python implementation of the Levenberg-Marquardt algorithm. For each relationship, the goodness-of-fit between the individual observations, O_i, and fitted model predictions, P_i, was characterized through the coefficient of determination R^2. To further assess model performance, scatterplots depicting model-derived versus measured values were subjected to Model II (reduced major axis) regression. We report values for the slope, intercept, and correlation coefficient R resulting from this analysis. Other statistical parameters of model performance include the median values of the ratio of model-derived to measured data, MdR, median values of the model bias, MdB = median ($P_i - O_i$), and the median absolute percent difference, $MdAPD = 100 \times \text{median}|P_i - O_i/O_i|$, between the model-derived and measured values. The root mean square deviation between model predictions and observations, $RMSD$, is also provided. This analysis was performed on the same data set that was used to parameterize the modeled relationships.

3. Results and Discussion

3.1. General Features of the PSD

Figure 2 illustrates the density functions for particle number, area, and volume concentration obtained for the entire data set (n = 168 observations). For some PSDs, portions of the density function exhibit rapid bin-to-bin variations that reflect poor counting statistics associated with low particle concentrations; this is generally most prevalent in the region $D > 20$ μm but also occasionally observed in the region $D = 2$ to 4.8 μm representing the range of the 30-μm aperture near the merge point with the 200-μm aperture. Particle number concentrations, $N'(D)$, in the smallest diameter size bins vary five orders of magnitude and range from 10^8 to more than 10^{13} m^{-3} μm^{-1}, while concentrations in the largest diameter size bins span the range 10^2 to more than 10^7 m^{-3} μm^{-1}. Particle area concentrations, $A'(D)$, in the smallest diameter size bins range from 10^8 to nearly 10^{13} μm^2 m^{-3} μm^{-1}, while concentrations in the largest size bins range from 10^{-5} to 10^9 μm^2 m^{-3} μm^{-1}. Particle volume concentrations, $V'(D)$, in the smallest diameter size bins range from 10^8 to more than 10^{11} μm^3 m^{-3} μm^{-1} while concentrations in the largest size bins range from fewer than 10^7 to nearly 10^{12} μm^3 m^{-3} μm^{-1}. The highest observed total concentrations generally occurred in coastal areas, plankton blooms, or near the bottom, while lower concentrations were generally associated with offshore areas or subsurface samples obtained below the chlorophyll a maximum but well above the bottom.

In all samples, the density functions of particle number, $N'(D)$, and area, $A'(D)$, concentration over the entire size range decreased in a generally logarithmic fashion with increasing diameter, and thus appear approximately linear when plotted with logarithmic scaling of both axes. This was also observed for nearly all density functions of particle volume, $V'(D)$, although three samples exhibited an increase in particle volume concentration with diameter. The calculated slopes ζ_N of $N'(D)$ range from −4.44 to −2.87 with an average value of −3.60 ± 0.33 (mean ± standard deviation) and a median value of −3.55 (Figure 3).

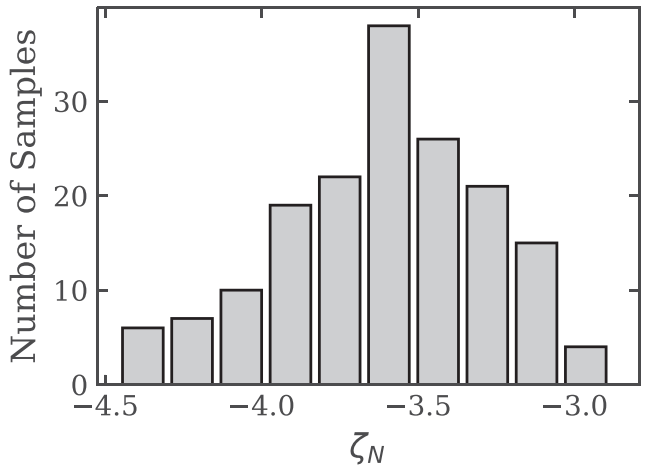

Figure 3. Histogram of the power law exponent ζ_N obtained by fitting a power law function to all measurements of $N'(D)$ (equation 2).

These average values and range of variability are consistent with previous studies of coastal and oceanic waters (Buonassissi & Dierssen, 2010; Jackson et al., 1997; Reynolds et al., 2010, 2016; Stemmann et al., 2008). Corresponding median values for the slopes ζ_A of $A'(D)$ and ζ_V of $V'(D)$ are −1.55 and −0.55, respectively. These values are in accordance with the assumption of spherical particles, for which $\zeta_A = \zeta_N - 2$ and $\zeta_V = \zeta_N - 3$, as discussed in Bader (1970).

Although the power law relationship may adequately characterize the overall relationship between particle abundance and size, significant departures from this model were observed in numerous samples from our data set. These consisted of discernible changes in the slope of the relationship for specific regions of the PSD, as well as obvious peaks in the distribution corresponding to specific particle, mostly likely planktonic, populations. Such features are illustrated in specific examples extracted from the data set.

Figure 4 depicts the measured density functions and corresponding cumulative distribution functions for samples representing the two extremes of particle mass concentration within our data set. The distributions shown in Figures 4a and 4b were obtained from a surface sample collected 9 km off the Alaskan coast near Utqiagvik (formerly known as Barrow). This extremely turbid sample (beam attenuation coefficient = 9.91 m^{-1} at 660 nm) exhibits the highest mass concentration of particles of any surface sample in the data set (SPM = 12.7 g m^{-3}). Despite the high SPM value, the particulate organic carbon content is low, and this sample exhibits the minimum POC/SPM value in our data set (0.024 g g^{-1}), suggesting that the sample is dominated by inorganic particles (Woźniak et al., 2010). The particle number size distribution for this sample is generally featureless with a steep overall slope across the distribution ($\zeta_N = -4.36$) indicating a proportionally high contribution of small particles to the PSD. However, deviations from the single slope obtained from the overall fit occur in portions of the size range

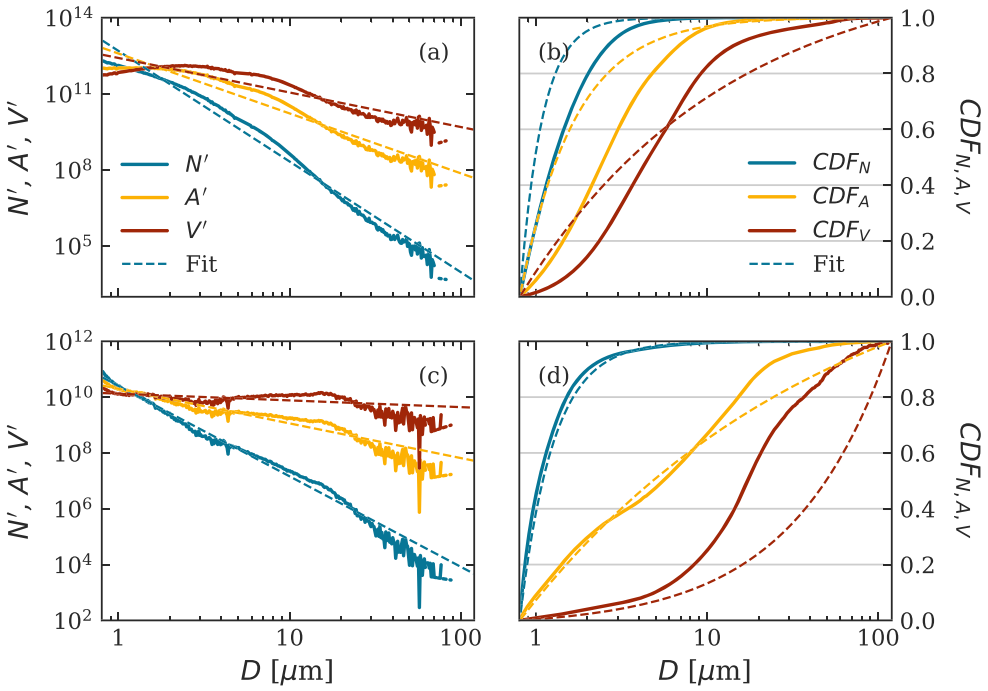

Figure 4. Example particle size distributions for samples representing the highest (a,b) and lowest (c,d) particle mass concentrations observed at near-surface depths. Panels (a,c) depict the measured distributions N', A', and V'; panels (b,d) depict the associated cumulative distribution functions, *CDF*. In all panels, dashed lines indicate the modeled distributions derived from a power law fit to the measured N'.

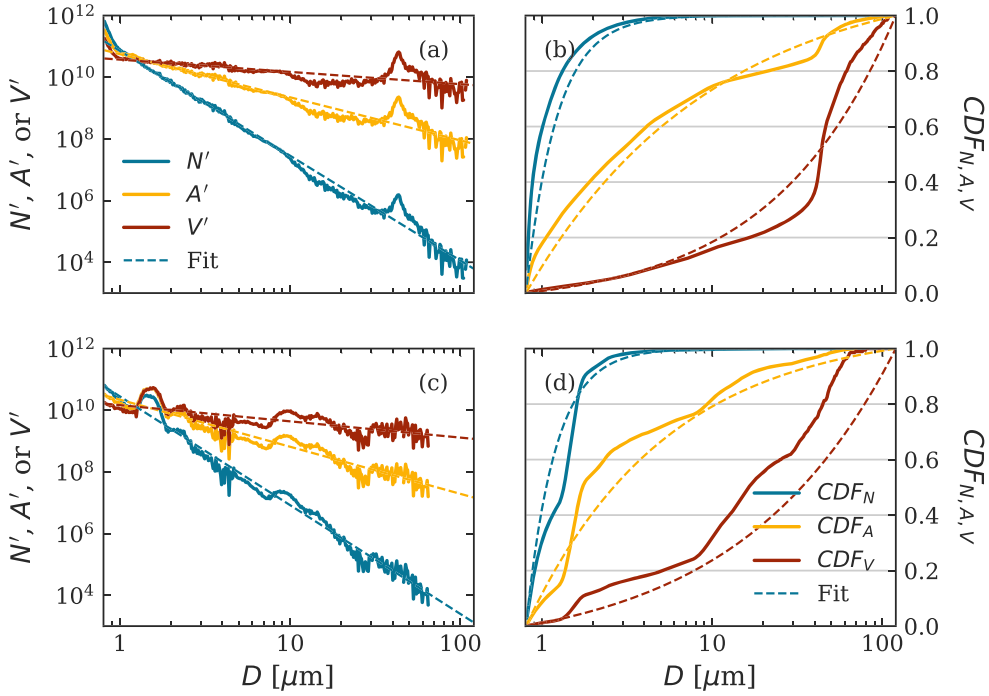

Figure 5. Similar to Figure 4, but for samples representing the subsurface chlorophyll *a* fluorescence maximum at two locations.

and these discrepancies are clearly discernable in a comparison of the cumulative distribution functions representing the measured $N'(D)$, $A'(D)$, and $V'(D)$ against those generated by the power law fit (Figure 4b). For example, the cumulative distribution function derived from the power law fit, $\widehat{CDF}_N$, is observed to overestimate the contribution of small particles resulting in an artificially steep cumulative distribution. This pattern becomes increasingly more pronounced in the power law predictions of the area and volume distribution and additionally illustrates that the power law model also overestimates the contribution of large particles.

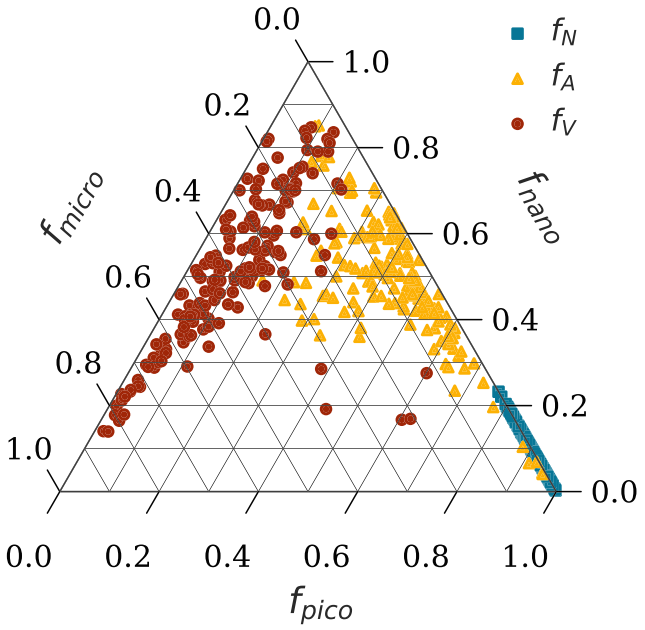

Figure 6. Ternary diagram illustrating the fractional contribution of three size classes (f_{pico}, f_{nano}, f_{micro}; equations 4a–4c) to the total concentration of particle number, N_t, cross-sectional area, A_t, and volume, V_t, as indicated by the legend.

In contrast, a sample obtained off the continental shelf in the western Beaufort Sea (Figures 4c and 4d) represents the lowest surface value of SPM obtained in our data set (0.044 g m^{-3}) and a relatively high POC/SPM ratio (0.47 g g^{-1}), suggesting that organic particles had a predominant contribution to particle mass concentration. This sample exhibits a flatter overall slope ($\zeta_N = -3.24$) than the example dominated by inorganic particles and has a discernable peak in the distribution centered near $D = 11$ μm (Figure 4c). This peak is also visible in Figure 4d as an increase in the slope of $CDF_A(D)$ and $CDF_V(D)$ in the same size range. The power law model provides a somewhat better description of the measured $N'(D)$ than in the sample illustrated in Figures 4a and 4b, as indicated by closer agreement between the $CDF_N(D)$ and the fitted line in Figure 4d. However, departures from the model are still evident upon examination of the $CDF_A(D)$ and $CDF_V(D)$. In the latter, the power law fit dramatically overestimates the contribution of large particles to volume concentration.

Figure 5 depicts the measured density functions and cumulative distribution functions for two samples collected from the subsurface

Table 2
Values of the Coefficient of Determination, R^2, for Relationships Between the Fractional Contributions of Three Size Classes to the Total Particle Number Concentration ($f_{N,pico}$, $f_{N,nano}$, $f_{N,micro}$), With the Corresponding Fractional Contributions to Total Particle Cross-Sectional Area ($f_{A,pico}$, $f_{A,nano}$, $f_{A,micro}$) and Volume ($f_{V,pico}$, $f_{V,nano}$, $f_{V,micro}$) Concentration

	$f_{A,pico}$	$f_{A,nano}$	$f_{A,micro}$	$f_{V,pico}$	$f_{V,nano}$	$f_{V,micro}$
$f_{N,pico}$	0.74			0.46		
$f_{N,nano}$		0.82			0.42	
$f_{N,micro}$			0.85			0.61

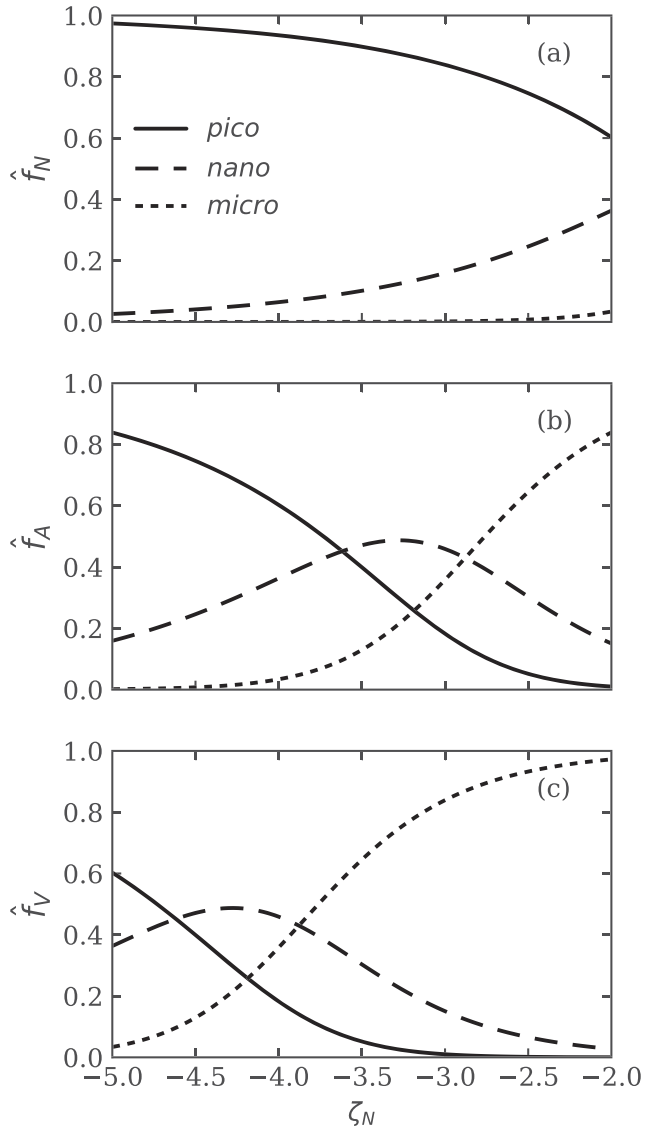

Figure 7. The theoretical fractional contributions of the picoplankton, $\hat{f}_{pico}$, nanoplankton, $\hat{f}_{nano}$, and microplankton, $\hat{f}_{micro}$, size classes to total particle (a) number, (b) cross-sectional area, and (c) volume concentration over the particle diameter range 0.8 to 120 μm calculated as a function of the power law slope ζ_N.

chlorophyll *a* fluorescence maximum. The particle assemblages in both samples are predominantly organic, with POC/SPM ratios exceeding 0.34. The distributions illustrated in Figures 5a and 5b are from a sample collected at a depth of 21 m in the Chukchi Sea. Phytoplankton pigment measurements indicate a high chlorophyll *a* concentration for this sample (2.3 mg m^{-3}) and suggest that the phytoplankton community was composed primarily of microplanktonic dinoflagellates, consistent with observation of a discrete peak in the PSD occurring near $D = 40$ μm (Figure 5a). In contrast, the distributions depicted in Figures 5c and 5d are from 56 m deep in the Beaufort Sea and with a much lower chlorophyll *a* concentration (0.5 mg m^{-3}). The phytoplankton community composition of this sample was largely composed of picophytoplankton species, consistent with a prominent peak in the size distribution centered near 1.6 μm (Figure 5c). This sample is additionally characterized by the presence of a second maximum around 10 μm and an additional feature around and above 30 μm, suggesting a diverse mix of plankton populations. Both samples shown in Figure 5 exhibit significant disagreements between the derived power law fits and measured data, such that the fitted values either overestimate or underestimate the measured data in different size ranges.

3.2. Relative Contributions of Size Classes to Particle Number, Area, and Volume Concentration

For each measured PSD, we quantified the fractional contribution of three different planktonic size ranges (f_{pico}, f_{nano}, and f_{micro}) to the total particle number, area, and volume concentration (Figure 6). In terms of particle number concentration, the contribution of the small-sized particles overwhelmingly dominates the numerical concentration with $f_{N,pico}$ averaging 90 ± 5.1% and always greater than 75%. The corresponding values of $f_{N,nano}$ range from 0.3% to 23%, with $f_{N,micro}$ never exceeding 0.2%. The fractional contributions of picoplankton and nanoplankton size classes to particle area concentration exhibit more variability than particle number with both $f_{A,pico}$ and $f_{A,nano}$ spanning a broad range (9–95% and 4–85%, respectively), while $f_{A,micro}$ again contributes only a relatively small fraction (8.5 ± 7.4%, always <35%). In contrast to particle number and area, the picoplankton size fraction has the smallest contributions to particle volume concentration ($f_{V,pico}$ in the range 1–62%, with only 7 samples >25%). The particle volume distribution is generally dominated by $f_{V,nano}$ (51 ± 17%) and $f_{V,micro}$ (39 ± 19%).

The fractional contribution of a size class in a given distribution, $N'(D)$, $A'(D)$, or $V'(D)$, is generally correlated with its contribution to other distributions. Table 2 summarizes the determination coefficients between size classes among the different measures of particle size. The contribution of the three size classes calculated from $N'(D)$ are more strongly correlated with the corresponding contributions determined from $A'(D)$ than with $V'(D)$. For example, the fractional contribution of the picoplankton size class to the total number concentration of particles, $f_{N,pico}$, is well correlated with its contribution to total particle area $f_{A,pico}$ ($R^2 = 0.74$) but to a lesser extent with its contribution to total particle volume $f_{V,pico}$ ($R^2 = 0.46$). The determination coefficients in Table 2 indicate that translating particle size classes from one measure of the PSD to another is not straightforward owing to the convolution of particle number and the area or volume weighting as a function of diameter.

3.3. Estimation of Particle Size Class Contributions From the Power Law Model

Figure 7 illustrates theoretical results obtained with calculations to show how varying the slope parameter of a single-slope power law model leads to changes in the predicted fractional contributions of the picoplankton, nanoplankton, and microplankton size classes to the total particle concentration in terms of number, area, and volume. In these calculations, the slope parameter ζ_N was varied between the values of −5 to −2, a broader range than observed in our field data set from the Arctic seas (Figure 3). The predicted picoplankton contribution to particle number concentration is dominant over the entire range of ζ_N, with contributions of the microplankton size class always low (<3.5%, Figure 7a). This pattern is consistent with our experimental data, in which $f_{N,micro}$ averaged about 0.03 ± 0.03% and never exceeded 0.18% (Figure 6). In contrast, for the volume distribution picoplankton are dominant only for the smallest (steepest) values of $\zeta_N \leq -4.75$, and microplankton contribute more than 50% over most of the range of ζ_N (Figure 7c). The patterns observed for the area concentration distribution are intermediate between the number and volume distributions (Figure 7b). Although the nanoplankton size fraction can be appreciable and even the largest contributor to area or volume over a narrow range of ζ_N, the value of $\hat{f}_{nano}$ never exceeds 0.5 in any of the three distributions.

We examined how well the single-slope power law approximation to our measurements of the particle number distribution predicts the fractional contributions of each size class to total particle number, area, and volume concentration. The fitted values of the slope parameter ζ_N (equation 2) determined from each

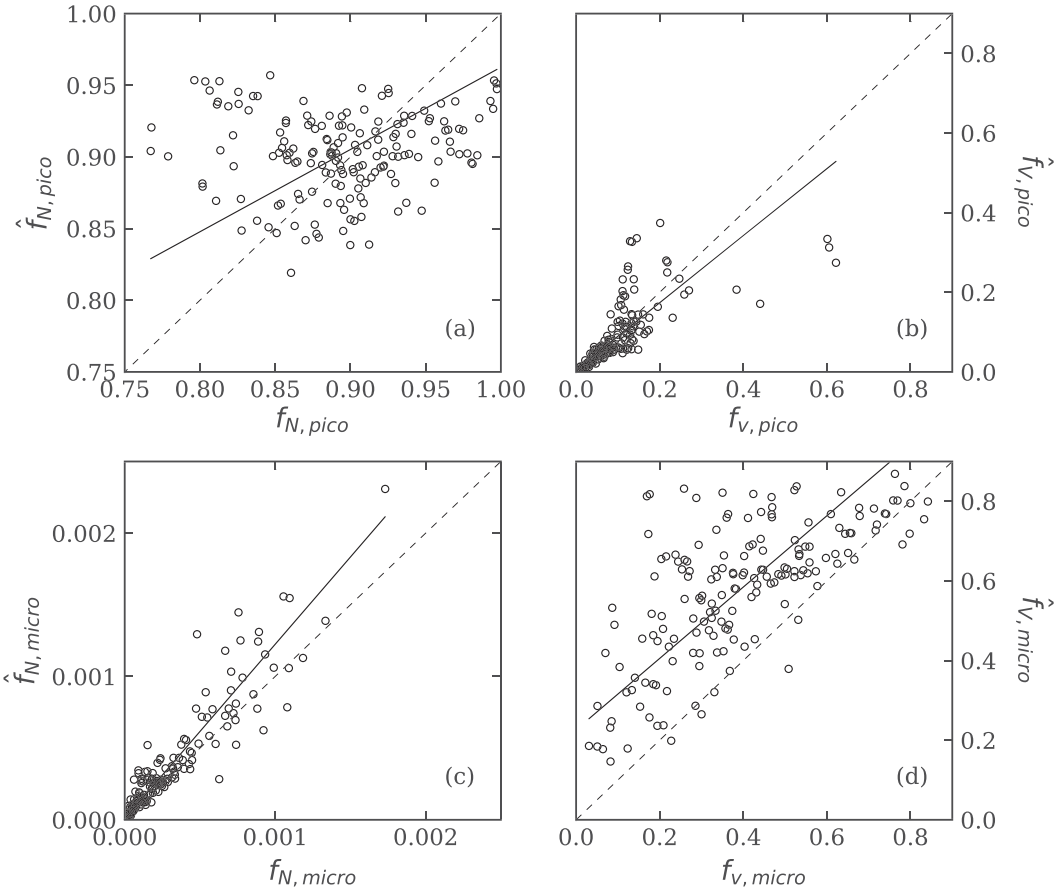

Figure 8. Scatter plots comparing measured values of the fractional contributions of picoplankton, f_{pico}, and microplankton, f_{micro}, size classes to those derived from a power law fit ($\hat{f}_{pico}$, $\hat{f}_{micro}$). (a,c) Fractional contribution to particle number concentration. (b,d) Fractional contribution to particle volume concentration. In each panel, the dashed line indicates the 1:1 line and the solid line represents the Model II regression line.

measured size distribution, $N'(D)$, were used to estimate the predicted (modeled) contribution of each size fraction ($\hat{f}_{N,pico}, \hat{f}_{N,nano}, \hat{f}_{N,micro}$). These modeled contributions were then compared with the actual contributions ($f_{N,pico}, f_{N,nano}, f_{N,micro}$) computed from equations 4a–4c using the measured data. Similar calculations were made on the basis of $A'(D)$ and $V'(D)$ distributions, which provided the comparison of modeled $\hat{f}_{A,pico}, \hat{f}_{A,nano}, \hat{f}_{A,micro}$ with measured $f_{A,pico}, f_{A,nano}, f_{A,micro}$ as well as the comparison of modeled $\hat{f}_{V,pico}, \hat{f}_{V,nano}, \hat{f}_{V,micro}$ with measured $f_{V,pico}, f_{V,nano}, f_{V,micro}$.

Scatter plots depicting four of these comparisons between the modeled and observed size class contributions are illustrated in Figure 8, and Table 3 provides a statistical evaluation for these relationships in addition to other comparisons not illustrated. In general, the correlations between the power law model predictions and actual observed values are strongest for the microplankton size class, that is, moderate to high correlation with the correlation coefficient R ranging from 0.68 for the particle volume distribution to 0.93 for the number distribution (Table 3, Figures 8c and 8d). However, the power law predictions of $\hat{f}_{N,micro}$, $\hat{f}_{A,micro}$, and $\hat{f}_{V,micro}$ are all characterized by significant positive bias (the median ratio of predicted to measured data, *MdR*, in the range 1.26 to 1.61) and relatively large values of median absolute percent difference between predicted and measured data (*MdAPD* between about 30% and 60%, Table 3). The weakest correlations between the power law model predictions and measured data are observed for the nanoplankton size class. Specifically, for these size fractions, the correlation coefficient R is always weak, ranging from 0.09 to 0.37 depending on the type of PSD (Table 3). For the picoplankton size class, the correlation between the power law predictions and measured data ranges from very weak ($R = 0.1$ for the particle number distribution; Figure 8a) to moderate or moderately high ($R = 0.63$ and 0.72 for area and volume distribution, respectively; Table 3). It is notable, however, that the case with moderately high correlation coefficient of 0.72 for the volume distribution is characterized by significant negative bias (*MdR* = 0.8) and increased *MdAPD* of 28% (Table 3, Figure 8b).

Overall, these results indicate that the role of the nanoplankton and microplankton size classes cannot be predicted well by the power law under any of the circumstances encountered in our data set, with typical prediction errors ranging from 16% to 61%. The best performance of the power law in terms of minimal error and bias is the prediction of the contribution of picoplankton size class to the particle number concentration; however, this represents a case in which picoplankton contribution is always dominant and the value of $\hat{f}_{N,pico}$ varies over a small range regardless of the power law slope. In addition, in this case, the correlation coefficient between the predicted $\hat{f}_{N,pico}$ and measured $f_{N,pico}$ is extremely low ($R = 0.1$). Thus, the general conclusion that stems from the analysis of our Arctic data set is that the power law fits to the measured PSDs do not provide acceptable estimates of the fractional contributions of picoplankton, nanoplankton, and microplankton size classes to total particle number, area, or volume concentration.

Table 3
Statistical Characterization of the Performance of a Power Law Model to Estimate the Fractional Contribution of Three Size Classes (f_{pico}, f_{nano}, f_{micro}) to the Particle Size Distribution Based on Particle Number (N), Cross-Sectional Area (A), and Volume (V) Concentration

Variable	Slope	Intercept	*R*	*MdR*	*MdB*	*MdAPD* [%]	*RMSD*
$f_{N,pico}$	0.57	0.39	0.10	1.00	<0.001	3.71	0.055
$f_{N,nano}$	0.57	0.04	0.09	1.00	<0.001	33.4	0.055
$f_{N,micro}$	1.22	0.00	0.93	1.26	<0.001	29.2	0.000
$f_{A,pico}$	0.86	0.08	0.63	1.02	0.005	16.0	0.128
$f_{A,nano}$	0.40	0.24	0.22	0.91	−0.044	18.2	0.151
$f_{A,micro}$	1.22	0.02	0.81	1.61	0.029	61.3	0.068
$f_{V,pico}$	0.84	0.01	0.72	0.80	−0.009	28.3	0.067
$f_{V,nano}$	0.56	0.05	0.37	0.69	−0.148	32.9	0.239
$f_{V,micro}$	0.90	0.23	0.68	1.51	0.158	50.5	0.235

Note. All comparisons are based on $n = 168$ measurements of the particle size distribution. Modeled values were determined by fitting the measured size distribution to a single slope power law function (equation 2) and calculating the predicted contributions of each size class. The slope, intercept, and correlation coefficient R of a Model II linear regression between modeled and measured variables is provided. Other statistical descriptors include the median ratio, *MdR*, median bias, *MdB*, and median absolute percent difference, *MdAPD*, between modeled and measured values. *RMSD* is the root mean square deviation. The values provided in rows 1, 7, 3, and 9 correspond to the relationships illustrated in Figures 8a to 8d, respectively.

3.4. Estimation of Particle Size Class Contributions From Percentiles of the Cumulative Distribution Functions

The cumulative distribution functions for particle number, $CDF_N(D)$, cross-sectional area, $CDF_A(D)$, and volume concentration, $CDF_V(D)$, obtained for all our measurements with equation 3 are depicted in Figure 9. For reference, predicted cumulative distribution functions, $\widehat{CDF}$, are also illustrated for the power law model with slopes of $\zeta_N = -4.5$, -3.5, and -2.5, which bracket the experimental median value of -3.55 obtained in this study. The $CDF_N(D)$ generally shows a rapid increase with increasing particle diameter as counts of large particles are always very low relative to the number of smaller particles. In contrast, the $CDF_A(D)$ and to greater extent the $CDF_V(D)$ show a less rapid increase, and generally a greater range in the

particle diameter associated with a given percentile as specified by a given value of $CDF_A(D)$ or $CDF_V(D)$. These patterns are evident from the size-dependent probability distributions of specific percentile values (Figure 10).

We examined relationships between specific percentile values of particle diameter obtained from the $CDF_N(D)$, $CDF_A(D)$, and $CDF_V(D)$ with the fractional contributions of the picoplankton, nanoplankton, and microplankton size classes to total particle concentrations N_t, A_t, and V_t (Table 4). This analysis aimed at identifying a relatively simple set of percentile diameters, which can serve as reasonable proxies for the contributions of the three particle size classes to diverse particulate assemblages encountered in natural waters, especially in the investigated Arctic waters. The median particle size has been previously used as a single descriptor of the PSD (e.g., Woźniak et al., 2010), but in our data set, this metric was generally a poor predictor of the three size class contributions with determination coefficients $R^2 < 0.6$ (see the values for $D_N(50)$, $D_A(50)$, and $D_V(50)$ in Table 4). The sole exception was that the median diameter based on the particle volume distribution, $D_V(50)$, was a reasonable predictor of the microplankton size class contribution to the total volume concentration, $f_{V,micro}$ ($R^2 = 0.85$).

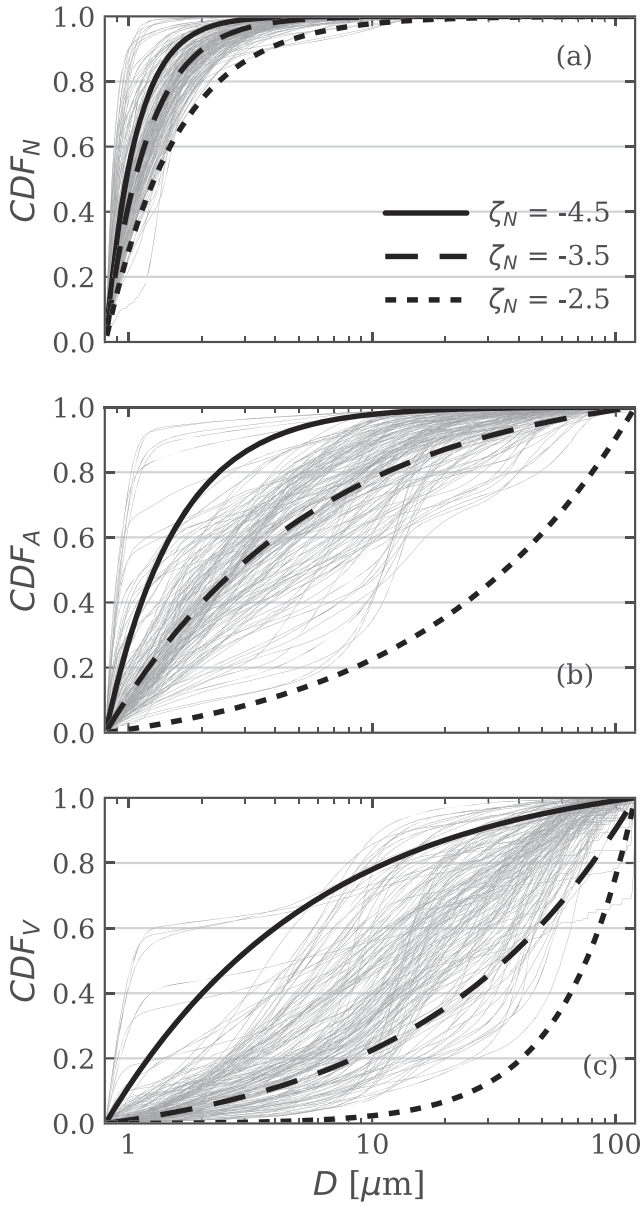

Figure 9. Measured cumulative distribution functions, *CDF*, of particle (a) number, (b) cross-sectional area, and (c) volume concentration. In each panel, all measured distributions are shown in gray and the distribution predicted by a power law model corresponding to different values of the slope ζ_N are shown for comparison.

The percentile diameters $D_N(80)$, $D_N(80)$, and $D_N(99.9)$ from the cumulative distribution $CDF_N(D)$ exhibited the highest determination coefficients with the respective size class contributions $f_{N,pico}$, $f_{N,nano}$, and $f_{N,micro}$ to the particle number concentration N_t (Table 4). The determination coefficients between all percentile diameters of the cumulative distribution function $CDF_A(D)$ with $f_{A,pico}$ and $f_{A,nano}$ were generally low and only $f_{A,micro}$ exhibited strong relationships, with the highest determination coefficient observed for $D_A(90)$ ($R^2 = 0.94$). Similarly, the microplankton contribution to the particle volume concentration, $f_{V,micro}$, was the only fraction demonstrating a high determination coefficient associated with percentiles derived from the cumulative distribution $CDF_V(D)$, with the percentile diameter $D_V(60)$ yielding the strongest relationship.

These four best-performing relationships, i.e. $f_{N,pico}$ versus $D_N(80)$, $f_{N,nano}$ versus $D_N(80)$, $f_{A,micro}$ versus $D_A(90)$, and $f_{V,micro}$ versus $D_V(60)$, are illustrated in Figure 11. The first three relationships are described by Model I linear regression models (Figures 11a–11c), while the fourth relationship is parameterized as a second-order polynomial function (Figure 11d). The fitted equations for these relationships are

$$\hat{f}_{N,pico} = -0.178\, D_N(80) + 1.17, \tag{5a}$$

$$\hat{f}_{N,nano} = 0.178\, D_N(80) - 0.17, \tag{5b}$$

$$\hat{f}_{A,micro} = 0.006\, D_A(90) - 0.02, \tag{5c}$$

$$\hat{f}_{V,micro} = -0.00012\, D_V(60)^2 + 0.020\, D_V(60) + 0.027. \tag{5d}$$

The size class contributions predicted by these relationships based on percentile diameters, $\hat{f}_{N,pico}$, $\hat{f}_{N,nano}$, $\hat{f}_{A,micro}$, $\hat{f}_{V,micro}$, are compared with measured values, $f_{N,pico}$, $f_{N,nano}$, $f_{A,micro}$, $f_{V,micro}$, in Figure 12. All four comparisons of modeled versus measured values exhibit high correlation ($R \geq 0.95$) with slope values of the Model II linear regression near one (Table 5). In addition, the statistics characterizing model bias and random error are all very good (Table 5) and greatly

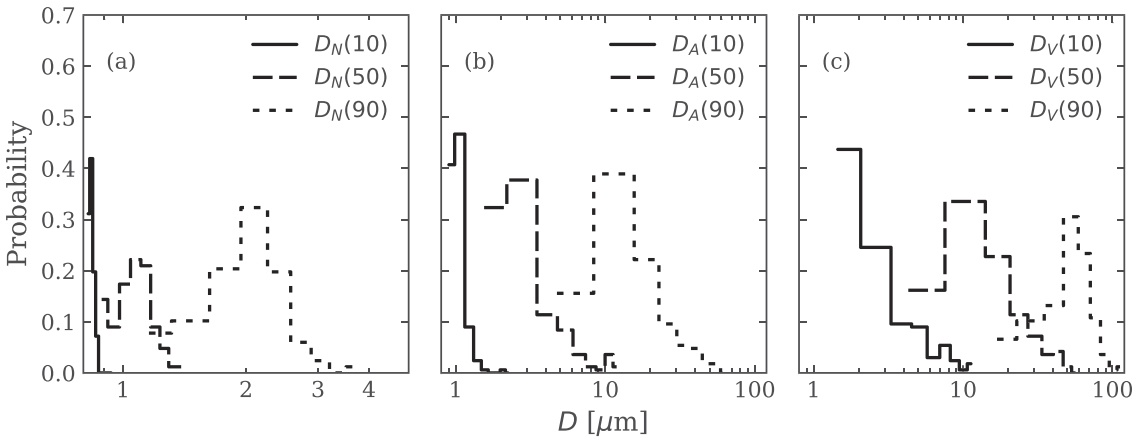

Figure 10. Frequency distributions of the particle diameter D representing the 10th, 50th, and 90th percentiles of the particle (a) number, (b) cross-sectional area, and (c) volume concentration. Note the different scaling of the x-axis in (a).

improved compared to the power law model results provided in Table 3. Specifically, the *MdR* values for the four relationships shown in Figure 11 indicate that the median bias is no greater than 1% and *MdAPD* generally less than 10%, with the highest value of only 13% for the case when $f_{N,nano}$ is predicted from $D_N(80)$ (Table 5). These results indicate that the use of specific percentile diameters derived from the cumulative distribution functions of particle size offers a highly promising approach for estimating the fractional contributions of diverse size classes, and warrants further investigation.

Table 4
Values of the Determination Coefficient, R^2, Between Diameters Representing Specific Percentiles (Given in Percent) of the Cumulative Distribution Function With the Corresponding Fractional Contributions of Three Size Classes to the Distribution

$CDF_N(D)$	$f_{N,pico}$	$f_{N,nano}$	$f_{N,micro}$	$CDF_A(D)$	$f_{A,pico}$	$f_{A,nano}$	$f_{A,micro}$	$CDF_V(D)$	$f_{V,pico}$	$f_{V,nano}$	$f_{V,micro}$
[μm]				[μm]				[μm]			
$D_N(1)$	<0.01	<0.01	<0.01	$D_A(1)$	0.30	0.38	<0.01	$D_V(1)$	0.23	0.01	0.11
$D_N(5)$	0.30	0.30	0.03	$D_A(5)$	0.45	0.47	0.01	$D_V(5)$	0.26	0.04	0.18
$D_N(10)$	0.36	0.36	0.01	$D_A(10)$	0.45	0.46	0.02	$D_V(10)$	0.32	0.11	0.34
$D_N(20)$	0.32	0.32	0.01	$D_A(20)$	0.37	0.36	0.03	$D_V(20)$	0.32	0.27	0.56
$D_N(25)$	0.37	0.37	0.01	$D_A(25)$	0.40	0.36	0.04	$D_V(25)$	0.30	0.33	0.62
$D_N(30)$	0.41	0.41	<0.01	$D_A(30)$	0.44	0.36	0.08	$D_V(30)$	0.29	0.38	0.67
$D_N(40)$	0.46	0.46	<0.01	$D_A(40)$	0.52	0.35	0.17	$D_V(40)$	0.28	0.46	0.77
$D_N(50)$	0.53	0.53	<0.01	$D_A(50)$	0.57	0.31	0.31	$D_V(50)$	0.28	0.54	0.85
$D_N(60)$	0.66	0.66	<0.01	$D_A(60)$	0.58	0.26	0.47	$D_V(60)$	0.25	0.59	**0.89**
$D_N(70)$	0.81	0.81	<0.01	$D_A(70)$	0.47	0.11	0.71	$D_V(70)$	0.18	0.63	0.86
$D_N(75)$	0.88	0.88	0.01	$D_A(75)$	0.38	0.05	0.81	$D_V(75)$	0.15	0.61	0.80
$D_N(80)$	**0.94**	**0.94**	0.02	$D_A(80)$	0.32	0.02	0.87	$D_V(80)$	0.10	0.56	0.69
$D_N(90)$	0.87	0.87	0.08	$D_A(90)$	0.26	<0.01	**0.94**	$D_V(90)$	0.04	0.52	0.57
$D_N(95)$	0.54	0.53	0.17	$D_A(95)$	0.23	<0.01	0.86	$D_V(95)$	0.04	0.43	0.49
$D_N(99)$	0.32	0.31	0.45	$D_A(99)$	0.13	<0.01	0.57	$D_V(99)$	0.04	0.23	0.27
$D_N(99.9)$	0.13	0.13	0.83	$D_A(99.9)$	0.04	0.01	0.31	$D_V(99.9)$	0.07	0.06	0.12

Note. Relationships between percentile diameters derived from the cumulative distribution of particle number concentration, $CDF_N(D)$, with the fractional contributions of picoplankton, $f_{N,pico}$, nanoplankton, $f_{N,nano}$, and microplankton, $f_{N,micro}$, size classes to the total particle number concentration are shown in columns 2 to 4. Similarly, relationships for the cumulative distributions of particle area, $CDF_A(D)$, and volume, $CDF_V(D)$, concentration are provided in columns 6 to 8 and columns 10 to 12, respectively. Values in boldface correspond to the four best-performing relationships given in equations 5a–5d and illustrated in Figure 11.

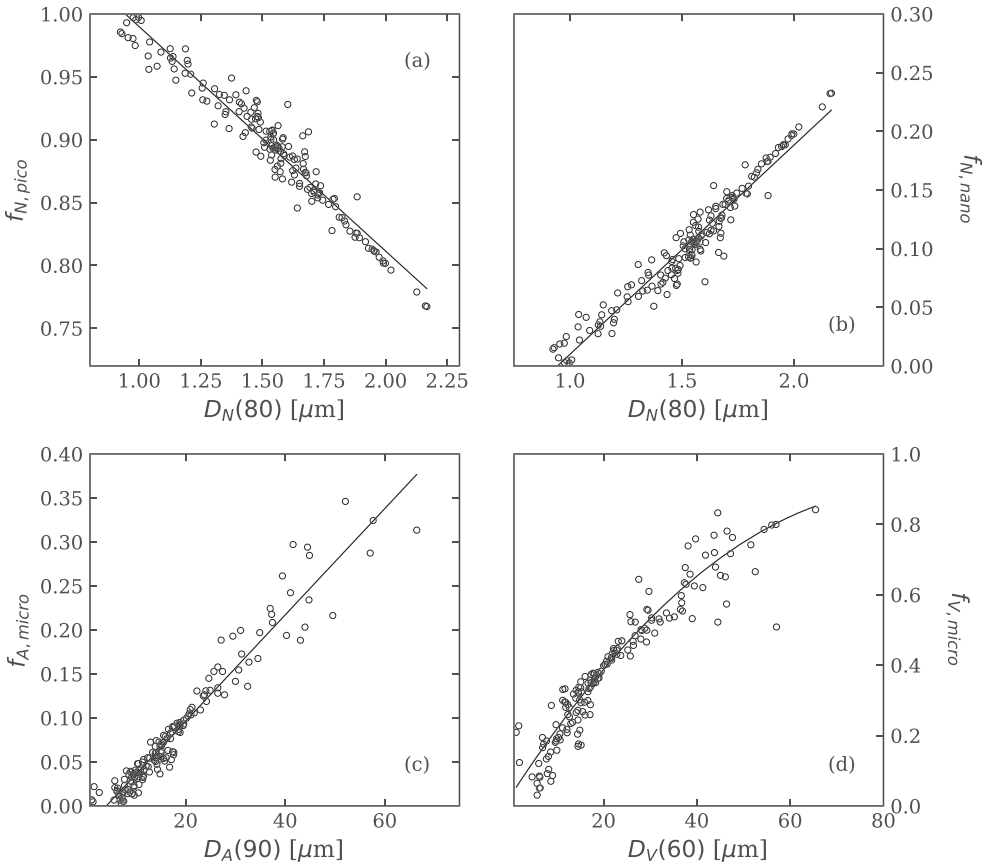

Figure 11. Example relationships between specific percentiles of the PSD and the fractional contribution of three size classes to the entire distribution. (a,b) Fractional contribution to total particle number concentration N_t of the picoplankton, $f_{N,pico}$, and nanoplankton, $f_{N,nano}$, size classes as a function of the 80th percentile particle diameter, $D_N(80)$. (c) Fractional contribution to total particle cross-sectional area concentration A_t of the microplankton size class, $f_{A,micro}$, as a function of the 90th percentile particle diameter, $D_A(90)$. (d) Fractional contribution to total particle volume concentration V_t of the microplankton size class, $f_{V,micro}$, as a function of the 60th percentile particle diameter, $D_V(90)$. The solid line in panels (a–c) depict a Model I linear regression fitted to the observations and in panel (d) depicts a fitted polynomial function obtained through a nonlinear least squares method.

The cumulative distribution functions depicted in Figure 9 indicate that the $CDF_V(D)$ exhibits the greatest range of variation between PSDs, followed by the $CDF_A(D)$ and then the $CDF_N(D)$. However, percentile values derived from $CDF_N(D)$ generally had strong determination coefficients with the fractional size class contributions, especially for picoplankton and nanoplankton size classes (Table 4). This is likely because all PSDs in our data set exhibited a very small value of $f_{N,micro}$ (Figure 6), so the problem of determining three size classes from a single variable was reduced to the simpler problem of predicting two classes ($f_{N,pico}$ and $f_{N,nano}$) that must sum to a value nearly equal to 1. Because $f_{V,pico}$ was also generally quite small, similar reasoning suggests that percentile diameters from the $CDF_V(D)$ should also show strong correlations with $f_{V,nano}$ and $f_{V,micro}$. Although relatively strong determination coefficients are observed with $f_{V,micro}$ (e.g., $R^2 \geq 0.8$ for diameters corresponding to 50th to 75th percentile range), similarly strong correlations are not seen for $f_{V,nano}$. This can be attributed to the observation that although values of $f_{V,pico}$ are generally small (10 ± 8%), they are still appreciably greater than zero so that the closure of the budget of contributions to particle volume concentration still requires an accurate estimation of three size classes.

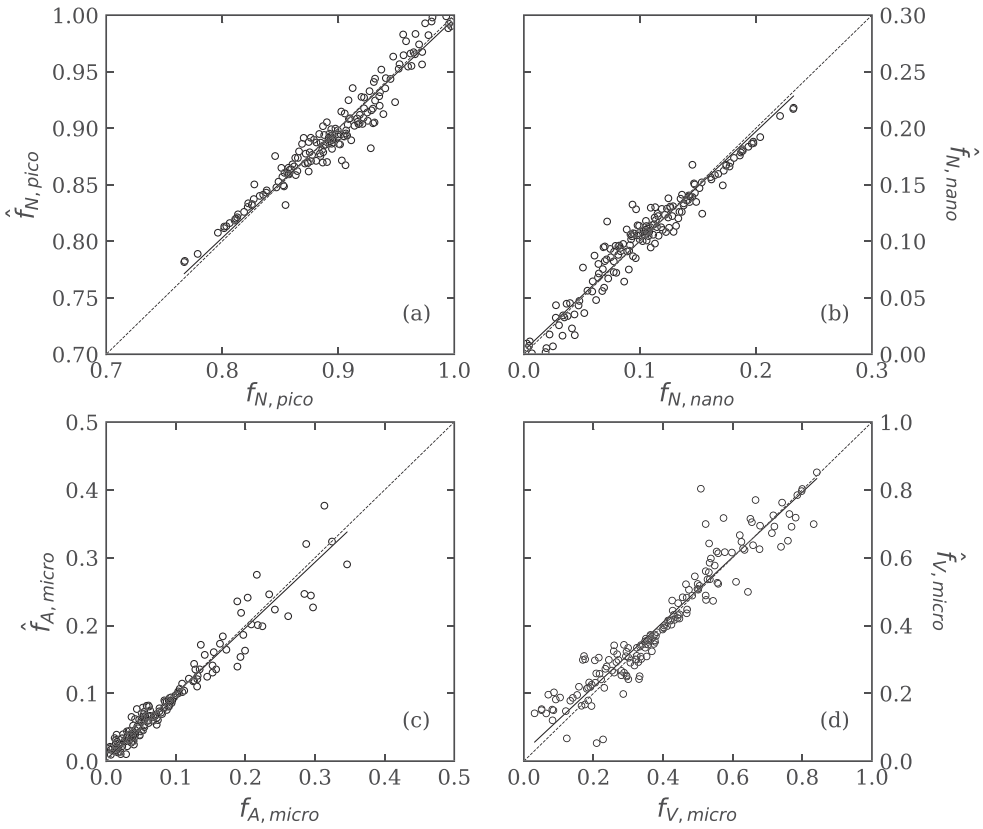

Figure 12. Comparison of model-derived with measured values for the relationships depicted in Figures 11a–11d and described in equations 5a–5d. In each panel, the dotted line represent the 1:1 line and the solid line represents the Model II regression line.

The determination coefficients for a given size fraction are observed to be generally highest at the percentile values where the range of corresponding diameters most closely match the diameter used to demarcate one size fraction from another and decrease as these values move further away from these limits. For example, the highest determination coefficient for $f_{V,micro}$ is observed with the 60th percentile diameter of the volume distribution, $D_V(60)$, so this percentile diameter was selected as the best proxy for predicting $f_{V,micro}$ (Table 4, Figure 11d). The mean value of $D_V(60)$ in our data set is 22.3 ± 13.3 μm, which is very close to the value of 20 μm that defines the lower boundary of the microplankton size range (Figure 13). Percentiles higher than 60% corresponded to diameters significantly larger than 20 μm, for example, the average value of $D_V(90)$ was 54.6 ± 19.9 μm. Thus, the portion of $CDF_V(D)$ corresponding to relatively high values of this function ($CDF_V(D) > 0.6$) carried more information about the distribution of particles within the microplankton size fraction than the magnitude of $f_{V,micro}$ relative to magnitudes of $f_{V,pico}$ and $f_{V,nano}$. Similar reasoning also explains why $D_N(80)$, which has an average value of 1.53 ± 0.3 μm (Figure 13), most accurately predicted the contributions $f_{N,pico}$ and $f_{N,nano}$ (Table 4, Figures 11a and 11b), and $D_A(90)$ with a value of 18.1 ± 11.9 μm (Figure 13) was the best proxy for predicting $f_{A,micro}$ (Table 4, Figure 11c). These results imply that different combinations of PSD size ranges and desired size intervals will result in different percentiles correlating best with those size classes.

Table 5
Similar to Table 3, but for Predicted Values Calculated From Percentiles of the Cumulative Distribution Function Using the Relationships in Equations 5a–5d

Variable	Slope	Intercept	R	MdR	MdB	$MdAPD$ [%]	$RMSD$
$f_{N,pico}$	0.97	0.03	0.97	1.00	0.001	0.89	0.0123
$f_{N,nano}$	0.97	<0.01	0.97	0.99	−0.001	7.84	0.0123
$f_{A,nano}$	0.97	<0.01	0.97	1.00	<0.001	13.35	0.0183
$f_{V,micro}$	0.96	0.03	0.95	1.01	0.005	7.48	0.0603

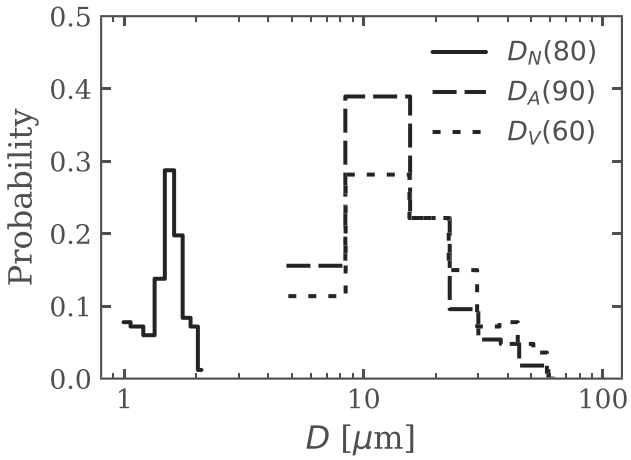

Figure 13. Frequency distribution of the three percentile diameters used in the relationships depicted in Figure 11.

4. Conclusions

Our measurements on seawater samples from the Arctic Ocean indicate that the size distribution of suspended particle assemblages in this environment exhibits a wide range of variation in both the magnitude and shape of the distribution of particle number, cross-sectional area, and volume concentration. The high size resolution of the Coulter Counter measurements reveals that changes in the slope of the size distribution generally occur over the measured size range of 0.8 to 120 μm, and additionally shows the frequent occurrence of peaks in the distribution associated with planktonic populations. In our data set, these deviations from an idealized single-slope power law parameterization are a consistent feature in nearly all measured size distributions of natural particle assemblages suspended in seawater.

Analysis of this data set was used to quantify the relative contributions of three particle size classes (picoplankton, nanoplankton, and microplankton) to the integrated size distribution. The number of particles per unit volume always exhibits an overall strong decrease with increasing particle diameter, and thus the contribution of particles in the picoplankton size range to the total number concentration of particles is always high (77% to 99%) and larger particles have only small contributions. The size distributions based on particle cross-sectional area and volume are characterized by an increasing contribution of nanoplankton and microplankton size classes at the expense of decreasing picoplankton contribution. Importantly, however, the complex and varied shapes exhibited by the PSD result in a large degree of variability among the contributions of the size classes to particle area and volume concentration and also limits the straightforward translation of a size class contribution from one distribution to another.

In many oceanic studies, simple one or two parameter models such as the power law distribution are used to describe the shape of the PSD in aquatic ecosystems. Our field measurements indicate that while a power law model may describe the overall general trend of the PSD in natural marine particle assemblages, significant departures from a single power law slope commonly occur throughout the size range. As a consequence, application of this model can yield considerable error in predicting the fractional contributions of individual size classes to the total number, area, or volume concentration.

Alternative metrics such as mean or median particle size have also been used as a simple means to characterize PSDs. We examined the utility of specific percentile diameters derived from the cumulative distribution function of particle number, area, or volume concentration to estimate the relative contribution of the three size classes to these distributions. Although median particle diameter was generally a poor predictor of size class contributions, other percentile diameters were observed to be strongly correlated with the contributions of individual size classes. These results suggest that the development and use of such metrics can lead to significantly improved estimates of individual size class contributions compared to the power law model. In this study, the best-performing percentile diameters for discriminating the contributions of different size classes were generally those which displayed a marked variation among individual PSDs, and exhibited a frequency distribution that straddled the diameter used to delineate individual size classes. For the particle size classes chosen in this study, these best-performing percentiles consisted of $D_N(80)$ for estimating both $f_{N,pico}$ and $f_{N,nano}$, $D_A(90)$ for the estimation of $f_{A,micro}$, and $D_V(60)$ for the estimation of $f_{V,micro}$. The choice of percentile diameters for developing a given approach will depend on the overall size range in question, as well as the desired size class definitions. These results expand on our previous studies of the optical properties of particle suspensions in which metrics such as $D_V(50)$ and $D_V(90)$ were used as indicators for the relative contributions of small and large particles (Koestner et al., 2020; Woźniak et al., 2010).

Our analysis utilizes size classes based on traditional size classifications of oceanic plankton (i.e., picoplankton, nanoplankton, microplankton), but it should be emphasized that our measurements encompass all particles suspended in seawater including living and nonliving particles, and both organic and minerogenic material. Although our analysis is based on measurements collected in Arctic seas, the wide diversity of particle assemblage types encountered in this region likely spans that of many marine habitats including the

pelagic, coastal, and estuarine environments. It is important to recognize, however, that the measured PSDs in this study are limited to a finite range of 0.8 to 120 μm, and thus contributions of smaller or larger particles outside of this size range are not assessed. Submicron particles (e.g., colloids or nanoparticles) as well as much larger particles (e.g., plankton chains or colonies, aggregates) can make a variable but significant contribution to both particle mass and size concentration in certain oceanic environments. In addition, marine particles can exhibit complex, nonspherical shapes that violate the assumptions employed in this study. The uncertainties in our results that arise from these limitations will depend on both the environment and the intended use of the PSD.

Optical measurements obtained from autonomous underwater vehicles or from above water platforms (e.g., aircraft and satellites) have the potential to extend observations of the PSD to the synoptic spatial and temporal scales necessary for studies of particle dynamics in the global ocean. Strong linkages between the PSD and the optical properties of seawater have long been recognized (e.g., Brown & Gordon, 1974; Jerlov, 1976; Kullenberg, 1974; Morel, 1973), and numerous studies have demonstrated relationships between specific metrics derived from the PSD with the light absorption and scattering characteristics of the particle suspension (Bowers et al., 2009; Briggs et al., 2013; Ciotti et al., 2002; Slade & Boss, 2015; Twardowski et al., 2001; Woźniak et al., 2010). These studies have typically utilized metrics such as mean or median particle size to characterize the PSD. Our results suggest that alternative metrics of the PSD, in particular, specific percentiles from the cumulative distribution functions of particle number, area, or volume concentration and chosen to target specific size class definitions, may provide a better means to represent the complex shape of the oceanic PSD. To take full advantage of this approach, further work is needed to establish quantitative relationships between these alternative percentile diameters and suitable proxies derived from measurements of seawater optical properties.

Acknowledgments

We thank Marcel Babin, Kevin Arrigo, Shigeto Nishino, Toru Hirawake, and all cruise participants for assistance in the field. Support for this work was provided by the National Aeronautics and Space Administration (NNX07AR20G, NNX10AG05G), the Japan Aerospace Exploration Agency (GCOM-C 311), and the National Science Foundation (OPP-1822021). Any opinions, findings, and conclusions or recommendations expressed in this study are those of the authors and do not necessarily reflect the views of these agencies. The authors declare no conflicts of interest with respect to the results of this paper. Data sets used in this study are publicly available in the LEFE-CYBER database (http://www.obs-vlfr.fr/proof/index2.php; MALINA cruise), the NASA SeaWiFS Bio-optical Archive and Storage System (https://seabass.gsfc.nasa.gov/; ICESCAPE 2010 and 2011 cruises), and the Data and Sample Research System for Whole Cruise Information database of the Japan Agency for Marine-Earth Sciences (https://doi.org/10.17596/0001879; MR1705-C cruise). We thank two anonymous reviewers for providing comments on the manuscript.

References

Agagliate, J., Lefering, I., & McKee, D. (2018). Forward modelling of inherent optical properties from flow cytometry estimates of particle size and refractive index. *Applied Optics*, *57*(8), 1777–1788. https://doi.org/10.1364/AO.57.001777

Agrawal, Y. C., & Pottsmith, H. C. (2000). Instruments for particle size and settling velocity observations in sediment transport. *Marine Geology*, *168*, 89–114. https://doi.org/10.1016/S00253227(00)00044-X

Bader, H. (1970). The hyperbolic distribution of particle sizes. *Journal of Geophysical Research*, *75*, 2822–2830. https://doi.org/10.1029/JC075i015p02822

Baker, E. T., & Lavelle, J. W. (1984). The effect of particle size on the light attenuation coefficient of natural suspensions. *Journal of Geophysical Research*, *89*, 8197–8203.

Bernard, S., Shillington, F. A., & Probyn, T. A. (2007). The use of equivalent size distributions of natural phytoplankton assemblages for optical modeling. *Optics Express*, *15*(5), 1995–2007. https://doi.org/10.1364/OE.15.001995

Bowers, D. G., Binding, C. E., & Ellis, K. M. (2007). Satellite remote sensing of the geographical distribution of suspended particle size in an energetic shelf sea. *Estuarine, Coastal and Shelf Science*, *73*, 457–466. https://doi.org/10.1016/j.ecss.2007.02.005

Bowers, D. G., Braithwaite, K. M., Nimmo-Smith, W. A. M., & Graham, G. W. (2009). Light scattering by particles suspended in the sea: The role of particle size and density. *Continental Shelf Research*, *29*, 1748–1755. https://doi.org/10.1016/j.csr.2009.06.004

Briggs, N. T., Slade, W. H., Boss, E., & Perry, M. J. (2013). Method for estimating mean particle size from high-frequency fluctuations in beam attenuation or scattering measurements. *Applied Optics*, *52*(27), 6710–6725. https://doi.org/10.1364/AO.52.006710

Brown, J. H., Gillooly, J. F., Allen, A. P., Savage, V. M., & West, G. B. (2004). Toward a metabolic theory of ecology. *Ecology*, *85*, 1771–1789. https://doi.org/10.1890/03-9000@10.1002

Brown, O. B., & Gordon, H. R. (1974). Size-refractive index distribution of clear coastal water particulates from light scattering. *Applied Optics*, *13*(12), 2874–2881. https://doi.org/10.1364/AO.13.002874

Brun-Cottan, J. C. (1971). Etude de la granulométrie des particules marines, mesures effectuées avec un compteur Coulter. *Cahiers Océanographiques*, *23*, 193–205.

Buonassissi, C. J., & Dierssen, H. M. (2010). A regional comparison of particle size distributions and the power law approximation in oceanic and estuarine surface waters. *Journal of Geophysical Research*, *115*, C10028. https://doi.org/10.1029/2010JC006256

Burd, A. B. (2013). Modeling particle aggregation using size class and size spectrum approaches. *Journal of Geophysical Research: Oceans*, *118*, 3431–3443. https://doi.org/10.1002/jgrc.20255

Carder, K. L., Beardsley, G. F. Jr., & Pak, H. (1971). Particle size distributions in the eastern equatorial Pacific. *Journal of Geophysical Research*, *76*, 5070–5077.

Chisholm, S. W. (1992). Phytoplankton size. In P. G. Falkowski, & A. D. Woodhead (Eds.), *Primary productivity and biogeochemical cycles in the sea*, (pp. 213–237). New York, N. Y: Plenum Press.

Ciotti, Á., Lewis, M. R., & Cullen, J. J. (2002). Assessment of the relationships between dominant cell size in natural phytoplankton communities and the spectral shape of the absorption coefficient. *Limnology and Oceanography*, *47*, 404–417. https://doi.org/10.4319/lo.2002.47.2.0404

Gillooly, J. F., Brown, J. H., West, G. B., Savage, V. M., & Charnov, E. L. (2001). Effects of size and temperature on metabolic rate. *Science*, *293*(5538), 2248–2251. https://doi.org/10.1126/science.1061967

Graham, G. W., & Nimmo-Smith, W. A. (2010). The application of holography to the analysis of size and settling velocity of suspended cohesive sediments. *Limnology and Oceanography: Methods*, *8*, 1–15.

Hansen, P. J., Bjørnsen, P. K., & Hansen, B. W. (1997). Zooplankton grazing and growth: Scaling within the 2-2,-μm body size range. *Limnology and Oceanography*, *42*, 687–704. https://doi.org/10.4319/lo.1997.42.4.0687

IOCCG (2014). Phytoplankton functional types from space. In S. Sathyendranath (Ed.), *Reports of the International Ocean Colour Coordinating Group*, (Vol. 15). Dartmouth, N.S: International Ocean Colour Coordinating Group. https://doi.org/10.1111/imre.12086

Jackson, G. A. (1995). Comparing observed changes in particle size spectra with those predicted using coagulation theory. *Deep-Sea Research Part II*, *42*, 159–184.

Jackson, G. A., Maffione, R., Costello, D. K., Alldredge, A. L., Logan, B. E., & Dam, H. G. (1997). Particle size spectra between 1 μm and 1 cm at Monterey Bay determined using multiple instruments. *Deep Sea Research Part I: Oceanographic Research Papers*, *44*, 1739–1767.

Jennings, S., & Warr, K. J. (2003). Smaller predator-prey body size ratios in longer food chains. *Proceedings of the Royal Society of London - Series B: Biological Sciences*, *270*(1522), 1413–1417. https://doi.org/10.1098/rspb.2003.2392

Jerlov, N. G. (1976). *Marine optics*. Amsterdam: Elsevier.

Jonasz, M. (1983). Particle-size distributions in the Baltic. *Tellus Series B: Chemical and Physical Meteorology*, *35*, 346–358. https://doi.org/10.3402/tellusb.v35i5.14624

Jonasz, M. (1987). Nonspherical sediment particles: Comparison of size and volume distributions obtained with an optical and a resistive particle counter. *Marine Geology*, *78*, 137–142. https://doi.org/10.1016/0025-3227(87)90072-7

Jonasz, M., & Fournier, G. (2007). *Light scattering by particles in water: Theoretical and experimental foundations*. San Diego, CA: Academic Press.

Kiefer, D. A., & Berwald, J. (1992). A random encounter model for the microbial planktonic community. *Limnology and Oceanography*, *37*, 457–467. https://doi.org/10.4319/lo.1992.37.3.0457

Kiørboe, T. (2000). Colonization of marine snow aggregates by invertebrate zooplankton: Abundance, scaling, and possible role. *Limnology and Oceanography*, *45*, 479–484. https://doi.org/10.4319/lo.2000.45.2.0479

Kiørboe, T., Grossart, H.-P., Ploug, H., Tang, K., & Auer, B. (2004). Particle-associated flagellates: Swimming patterns, colonization rates, and grazing on attached bacteria. *Aquatic Microbial Ecology*, *35*, 141–152. https://doi.org/10.3354/ame035141

Kitchen, J. C., Menzies, D., Pak, H., & Zaneveld, J. R. V. (1975). Particle size distributions in a region of coastal upwelling analyzed by characteristic vectors. *Limnology and Oceanography*, *20*, 775–783.

Knap, A. H., Michaels, A., Close, A. R., Ducklow, H., & Dickson, A. G. (1996). *Protocols for the Joint Global Ocean Flux Study (JGOFS) core measurements (Vol. 19). Reprint of the IOC Manuals and Guides (Vol. 29)*. Paris: UNESCO.

Koestner, D., Stramski, D., & Reynolds, R. A. (2020). Assessing the effects of particle size and composition on light scattering through measurements of size-fractionated seawater samples. *Limnology and Oceanography*, *65*, 173–190. https://doi.org/10.1002/lno.11259

Kostadinov, T. S., Siegel, D. A., & Maritorena, S. (2009). Retrieval of the particle size distribution from satellite ocean color observations. *Journal of Geophysical Research*, *114*, C09015. https://doi.org/10.1029/2009JC005303

Kostadinov, T. S., Siegel, D. A., & Maritorena, S. (2010). Global variability of phytoplankton functional types from space: Assessment via the particle size distribution. *Biogeosciences*, *7*, 3239–3257. https://doi.org/10.5194/bg-7-3239-2010

Kullenberg, G. (1974). Observed and computed scattering functions. In N. G. Jerlov, & E. Steeman-Nielsen (Eds.), *Optical aspects of oceanography*, (pp. 25–45). London: Academic Press.

Le Quéré, C., Harrison, S. P., Prentice, I. C., Buitenhuis, E. T., Aumont, O., Bopp, L., et al. (2005). Ecosystem dynamics based on plankton functional types for global ocean biogeochemistry models. *Global Change Biology*, *11*, 2016–2040. https://doi.org/10.1111/j.1365-2486.2005.1004.x

Moore, C., Barnard, A., Fietzek, P., Lewis, M. R., Sosik, H. M., White, S., & Zielinski, O. (2009). Optical tools for ocean monitoring and research. *Ocean Science*, *5*, 661–684.

Morel, A. (1973). Diffusion de la lumière par les eaux de mer; résultats expérimentaux et approche théorique. AGARD Lect. Ser., 3.1.1.–3.1.76. North Atlantic Treaty Organization.

Morel, A., & Bricaud, A. (1986). Inherent optical properties of algal cells including picoplankton: Theoretical and experimental results. *Canadian Bulletin of Fisheries and Aquatic Sciences*, *214*, 521–559.

Mouw, C. B., Hardman-Mountford, N. J., Alvain, S., Bracher, A., Brewin, R. J. W., Bricaud, A., et al. (2017). A consumer's guide to satellite remote sensing of multiple phytoplankton groups in the global ocean. *Frontiers in Marine Science*, *4*, 41. https://doi.org/10.3389/fmars.2017.00041

Parsons, T. R. (1969). The use of particle size spectra in determining the structure of a plankton community. *Journal of the Oceanographic Society of Japan*, *25*, 172–181.

Parsons, T. R., Maita, Y., & Lalli, C. M. (1984). *A manual of chemical and biological methods for seawater analysis*. Oxford, England: Pergamon Press.

Picheral, M., Guidi, L., Stemmann, L., Karl, D. M., Iddaoud, G., & Gorsky, G. (2010). The Underwater Vision Profiler 5: An advanced instrument for high spatial resolution studies of particle size spectra and zooplankton. *Limnology and Oceanography: Methods*, *8*, 462–473.

Platt, T., & Denman, K. L. (1978). The structure of pelagic marine ecosystems. *Conseil permanent international pour l'exploration de la mer, première réunion*, *173*, 60–65.

Ploug, H., & Grossart, H.-P. (2000). Bacterial growth and grazing on diatom aggregates: Respiratory carbon turnover as a function of aggregate size and sinking velocity. *Limnology and Oceanography*, *45*, 1467–1475. https://doi.org/10.4319/lo.2000.45.7.1467

Reynolds, R. A., Stramski, D., & Neukermans, G. (2016). Optical backscattering of particles in Arctic seawater and relationships to particle mass concentration, size distribution, and bulk composition. *Limnology and Oceanography*, *61*, 1869–1890. https://doi.org/10.1002/lno.10341

Reynolds, R. A., Stramski, D., Wright, V. M., & Woźniak, S. B. (2010). Measurements and characterization of particle size distributions in coastal waters. *Journal of Geophysical Research*, *115*, C08024. https://doi.org/10.1029/2009JC005930

Risović, D. (1993). Two-component model of sea particle size distribution. *Deep Sea Research Part I: Oceanographic Research Papers*, *40*, 1459–1473. https://doi.org/10.1016/0967-0637(93)90123-K

Sheldon, R. W., Prakash, A., & Sutcliffe, W. H. Jr. (1972). The size distribution of particles in the ocean. *Limnology and Oceanography*, *17*, 327–340.

Shi, W., & Wang, M. (2019). Characterization of suspended particle size distribution in global highly turbid waters from VIIRS measurements. *Journal of Geophysical Research: Oceans*, *124*, 3796–3817. https://doi.org/10.1029/2018JC014793

Sieburth, J. M., Smetacek, V., & Lenz, J. (1978). Pelagic ecosystem structure: Heterotrophic compartments of the plankton and their relationship to plankton size fractions. *Limnology and Oceanography*, *23*, 1256–1263. https://doi.org/10.4319/lo.1978.23.6.1256

Slade, W. H., & Boss, E. (2015). Spectral attenuation and backscattering as indicators of average particle size. *Applied Optics*, *54*(24), 7264–7277. https://doi.org/10.1364/AO.54.007264

Stemmann, L., & Boss, E. (2012). Plankton and particle size and packaging: From determining optical properties to driving the biological pump. *Annual Review of Marine Science*, *4*, 263–290. https://doi.org/10.1146/annurev-marine-120710-100853

Stemmann, L., Eloire, D., Sciandra, A., Jackson, G. A., Guidi, L., Picheral, M., & Gorsky, G. (2008). Volume distribution for particles between 3.5 to 2000 μm in the upper 200 m region of the South Pacific gyre. *Biogeosciences*, *5*, 299–310. https://doi.org/10.5194/bg-5-299-2008

Stemmann, L., Jackson, G. A., & Ianson, D. (2004). A vertical model of particle size distributions and fluxes in the midwater column that includes biological and physical processes — Part I model formulation. *Deep Sea Research Part I: Oceanographic Research Papers*, *51*, 865–884.

Stramski, D., Bricaud, A., & Morel, A. (2001). Modeling the inherent optical properties of the ocean based on the detailed composition of planktonic community. *Applied Optics*, *40*(18), 2929–2945. https://doi.org/10.1364/ao.40.002929

Stramski, D., & Kiefer, D. A. (1991). Light scattering by microorganisms in the open ocean. *Progress in Oceanography*, *28*, 343–383. https://doi.org/10.1016/0079-6611(91)90032-H

Twardowski, M. S., Boss, E., Macdonald, J. B., Pegau, W. S., Barnard, A. H., & Zaneveld, J. R. V. (2001). A model for estimating bulk refractive index from the optical backscattering ratio and the implications for understanding particle composition in case I and case II waters. *Journal of Geophysical Research*, *106*, 14,129–14,142.

van der Linde, D.W. (1998). Protocol for the determination of total suspended matter in oceans and coastal zones (technical note I.98.182). Ispra, Italy: Joint Research Centre.

Ward, B. A., Dutkiewicz, S., Jahn, O., & Follows, M. J. (2012). A size-structured food-web model for the global ocean. *Limnology and Oceanography*, *57*, 1877–1897. https://doi.org/10.4319/lo.2012.57.6.1877

Woodward, G., Ebenman, B., Emmerson, M., Montoya, J. M., Olesen, J. M., Valido, A., & Warren, P. H. (2005). Body size in ecological networks. *Trends in Ecology & Evolution*, *20*(7), 402–409. https://doi.org/10.1016/j.tree.2005.04.005

Woźniak, S. B., Stramski, D., Stramska, M., Reynolds, R. A., Wright, V. M., Miksic, E. Y., et al. (2010). Optical variability of seawater in relation to particle concentration, composition, and size distribution in the nearshore marine environment at Imperial Beach, California. *Journal of Geophysical Research*, *115*, C08027. https://doi.org/10.1029/2009JC005554

Xi, H., Larouche, P., Tang, S., & Michel, C. (2014). Characterization and variability of particle size distributions in Hudson Bay, Canada. *Journal of Geophysical Research: Oceans*, *119*, 3392–3406. https://doi.org/10.1002/2013JC009542